# Analytical Circuit-based Model for Low Thickness Tunable Metasurfaces Design

**P. Ropa and C. Legrand**
Unité de Dynamique et Structure des Matériaux Moléculaires, Université du Littoral-Côte d'Opale, Calais, 50 Rue F. Buisson, 62228, Calais, France

Corresponding author: First C. Legrand (e-mail: legrand@ univ-littoral.fr).

**ABSTRACT** An analytical model of metasurfaces made of a rectangular array deposited on a low thickness (10-150 µm) grounded dielectric layer is presented. The surface impedance and the equivalent circuit are extracted from full wave simulations. Contrary to previous works on higher thickness metasurfaces, the absorption corresponds to the first resonance under the patch. The equivalent circuit is made of a parallel resonant RLC circuit in series with an inductance $L_s$. The analytical expressions of the RLC components and of the quality factors are established from the study of the influence of the different parameters. The inductance $L_s$ is attributed to the non-metallized part of the mesh. The impedance of the resonant circuit expresses as the product of a proportionality factor, the impedance of a single patch and a periodicity factor. The model is validated on different examples. Specific properties are evidenced like the quasi-independence of the equivalent circuit resistance versus the length of the patch, the total absorption condition and the extension of the model to a two patches metasurfaces. Giving a better understanding of the role of the different parameters, the model is useful in view of new applications development notably electrically driven tunable metasurfaces.

**INDEX TERMS** metasurfaces, fully analytical model, rectangular patch, rectangular mesh, absorbers, high impedances surfaces, low thickness substrate.

## I. INTRODUCTION

METASURFACES are thin (2D) metamaterials consisting of periodic or non-periodic arrangement of identical or distinct planar electromagnetic microstructures. This structuration of the surface gives them specific properties for the control and the manipulation of the scattering of electromagnetic waves [1]- [3]. A large variety of structures covering a large field of applications from microwaves to optics through THz frequencies [4]- [6] were developed like for example frequency selective surfaces (FSS) [7]- [10], high impedance surfaces (HIS) [11]- [19], thin and perfect absorbers [20]- [24].

The rise of wireless telecommunications has generated growing interest in tunable and reconfigurable metasurfaces [25]- [26]. Such devices can be made tunable in order to adjust their working frequency; in this objective, one solution consists to use active materials with properties that can be modified by applying an external action. Nematic liquid crystals are one of this materials type [27]. In fact, inserted between two close electrodes (thickness in the range 5 to several hundred µm), their permittivity can be continuously driven with an external electric field of moderate amplitude (0.1 V/µm). These materials have been experimented as promising active materials in tunable microwave and millimeter devices and applications [28]- [31]; they present other advantages like a low microwave permittivity ($\varepsilon' \approx 3$), an available implementation technology including flexible substrates and a reduced turn-off response time at low thickness. In order to analyze the behavior of liquid crystal based metasurfaces, it's important to develop models considering the low thickness of such structures.

In the present paper, we propose an analytical model for low thickness periodic patch array metasurfaces. Such structures were largely studied [11]- [23] notably after the work of D. Sievenpiper [11]- [13] proposing their use as high impedance surface (HIS). In these different works, the effective circuit model is a parallel LC circuit (excepted in [22] where a RLC series circuit is used for the patch array giving similar behaviors) corresponding to the resonance appearing at the gap between two neighboring patches (Fig. 5.1.2 of [11]). The analytical model based on the averaged expressions for FSS impedance is sufficiently accurate only for thick dielectrics [14], [16], [32]; this results from the assumption that only the fundamental-mode plane wave propagates between the array and the ground [16]- [17].

In the case of low/very low thickness, the resonance occurs under the patch and the electric field is orientated perpendicular to the ground plane in this part (TM mode). Few studies have concerned this case [33] for which previous models don't apply.

The main originality of this work is to propose an analytical expression of each RLC$L_s$ circuit elements as a function of the geometrical (l, w, t, $p_l$, $p_w$) and substrate (ε', tgδ)

parameters. No previous simulation is necessary. To our knowledge, such a model has never been proposed. The total absorption condition as a function of the different parameters is also deduced. The choice of rectangular patches and/or mesh offers an additional degree of freedom (patch width, transversal period) for the metasurface properties adjustment to specifications [34]. Analytical models [16], [35]- [37] tend to drastically reduce the calculation time and lead to a better insight and understanding on the device operation and on the influence of the different parameters. This is useful to guide the configuration of the device. As previously mentioned, the analytical modelisation of low thickness metasurfaces is of interest as such metasurfaces allow the electrical driving of active materials (LC, thin film ferroelectrics ...) and offers a possibility to design tunable metasurfaces.

## II. MODELIZED STRUCTURE

The studied metasurface is a 2-D periodic distribution of rectangular metal patches on a thin and low losses dielectric layer (permittivity ε', dielectric losses factor tgδ = ε"/ε', ε" dielectric losses) short-circuited by a ground plane (Fig. 1). The mesh is also rectangular. The incident electromagnetic wave is considered at normal incidence and polarized along the length *l* of the patch (Ox axis).

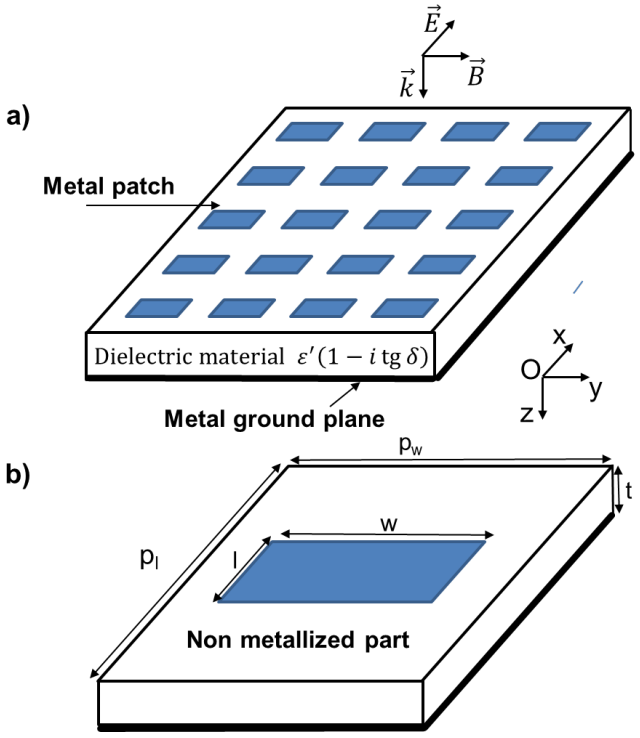


**FIGURE 1**. (a) General view of the modeled structure, (b) The unit cell (structure mesh). The structure dimensions are the width w, the length l of the patch (along the field direction) and the periods $p_w$ and $p_l$ of the array. The parameters *t*, *ε'*, *tgδ* = ε"/ε', ε" represent respectively the thickness, the real permittivity, the dielectric losses factor and the dielectric losses of the dielectric substrate.

The metasurface is characterized by the reflection coefficient $S_{11}(F)$ and the surface impedance $Z(F)$ in the input plane ($z$ = 0). These two quantities are connected via the classical formula:

$$Z(F) = Z_0 \frac{1+S_{11}(F)}{1-S_{11}(F)} \qquad Z_0 = \sqrt{\frac{\mu_0}{\varepsilon_0}} = 120\pi = 377\,\Omega \tag{1}$$

where $Z_0$ represents the impedance of free space. Each patch constitutes with the ground plane and the dielectric substrate a micro-strip line of length *l* (Fig. 1.b) which behaves as a resonator. It is known that the incident electric field induces a charge distribution on the surfaces of the patch as well as on the ground plane resulting in an electric field under the patch orientated along the Oz direction [33], [40]- [42]. This electric field is reinforced with the small thickness *t* of the dielectric substrate. Such a configuration is favorable to TM modes propagation under the patch along Ox. These modes are reflected at each edge of the patch and a standing wave is formed. As a consequence, resonance phenomena appear at specific wavelengths $\lambda_{Rn}$ and frequencies $F_{Rn}$ [40], [41]:

$$\lambda_{Rn} = \frac{2l_{eff}\sqrt{\varepsilon'_{eff}}}{(2n+1)} \qquad F_{Rn} = \frac{(2n+1)c}{2l_{eff}\sqrt{\varepsilon'_{eff}}} \tag{2}$$

Where c is the celerity, n is a whole number, $\varepsilon'_{eff}$ and $l_{eff}$ are respectively the effective permittivity and the effective length of the patch. These effective parameters are introduced to consider the fringing effects and the dispersion of the micro-strip line (see VIII. Appendix). At the resonance frequencies, the signal phase shift after a round trip of length $2l_{eff}$ is a multiple of 2π so the wave comes back in phase. In this work, only the first resonance ($n$ = 0) will be considered:

$$\lambda_{R0} = 2l_{eff}\sqrt{\varepsilon'_{eff}} \qquad F_{R0} = \frac{c}{2l_{eff}\sqrt{\varepsilon'_{eff}}} \tag{3}$$

At the vicinity of each resonance, the modulus of the reflection coefficient can strongly decrease or not depending of losses. In case of no losses, no absorption is observed whereas the phase of the reflection coefficient goes abruptly from +π to -π. The metasurface behaves as an HIS [10]- [17] known as artificial magnetics conductors (AMCs) and to reduce effects of surface waves. Such structures are used as ground planes for antenna performance improvement and miniaturization and also to improve computational efficiency.

In case of dielectric/metallic losses, at the vicinity of the resonance, a part of the power is dissipated and the metasurface behaves as an absorber. A total absorption (perfect absorber) can also be obtained [23], [24], [33], [38]. Wideband and perfect absorbers were achieved using respectively the intrinsic loss of commercial substrates, lumped resistors or thin conductive inks [22].

The frequency tunability of such structures can be achieved using an electrically active material as the dielectric substrate and adding non-perturbing interconnections for the control of the substrate permittivity. Such tunable metasurfaces are interesting from applications point of view.

## III. REFLECTION COEFFICIENT AND SURFACE IMPEDANCE FROM FULL WAVE SIMULATIONS

In this section, the reflection coefficient $S_{11}(F)$ in the input plane is obtained from full wave simulations using COMSOL software based on the finite elements method. For these simulations, PEC and PMC limit conditions were used. The surface impedance $Z(F)$ is then calculated from the reflection coefficient $S_{11}(F)$ using (1). An example of typical frequency behavior for the reflection coefficient and the surface impedance is given respectively in Fig. 2 and Fig. 3. For this example, the first ( $n = 0$ ) resonance frequency $F_{R0}$ = 34.25 GHz ( $\varepsilon'_{eff}$ =2.95, $l_{eff}$ = 2.55 mm) is in the middle of the Ka band. The substrate thickness is very low ($t$ = 50 µm) compared to the wavelength in the dielectric substrate ($\lambda/\lambda_d$ > 100 with $\lambda_d=\lambda_0/\sqrt{\varepsilon'}$ where $\lambda_d$ represents the wavelength in the dielectric substrate). The dielectric losses are low ($tg\delta$ = 0.014). The metallic losses are not considered in this work (infinite conductivity of the metal parts). At low and high frequencies, the metasurface behaves as a reflector ($S_{11}(F) \approx$ -1, Fig. 2a). A minimum of the reflection coefficient modulus is observed at the frequency noted $F_{Rp}$ = 34 GHz ($|S_{11}|_{min}$ = -11.8 dB, Fig. 2b,

index p for parallel resonance) near $F_{R0}$ (-0.76%,). This behavior can be attributed as previously described to the first resonance under the patch. The resonance phenomenon is confirmed by the polar plot of the reflection coefficient $S_{11}(F)$ which describes a circle (Fig. 2a).

Concerning the surface impedance $Z(F)$, its imaginary part (Fig. 3a) anneals ($Z(F)$ real) and changes sign two times in the studied frequency range: at the frequency $F_{Rp}$ and at a higher frequency noted $F_{Rs}$ = 37.8 GHz (index s for series resonance). The impedance is inductive at low and high frequencies (Im($Z(F)$) > 0) and capacitive between $F_{Rp}$ and $F_{Rs}$ (Im($Z(F)$) < 0). At $F_{Rp}$, Re($Z(F)$) is maximum whereas it is minimum at $F_{Rs}$. These behaviors are characteristic respectively of a parallel resonance at $F_{Rp}$ and of a series resonance at $F_{Rs}$ of the surface impedance. Such curves were already reported [32], [33] notably for dielectric resonators [38].

## IV. EQUIVALENT CIRCUIT AND DATA EXTRACTION METHOD

From these previous results, the equivalent circuit presented in Fig. 4 is proposed to model the surface impedance $Z(F)$ of the metasurface. It is constituted of a RLC resonant circuit in series with an inductance $L_s$ (index s for an inductance in series with the RLC parallel circuit). This electrical circuit exhibits the previously found properties: the circuit is inductive at low and high frequencies,

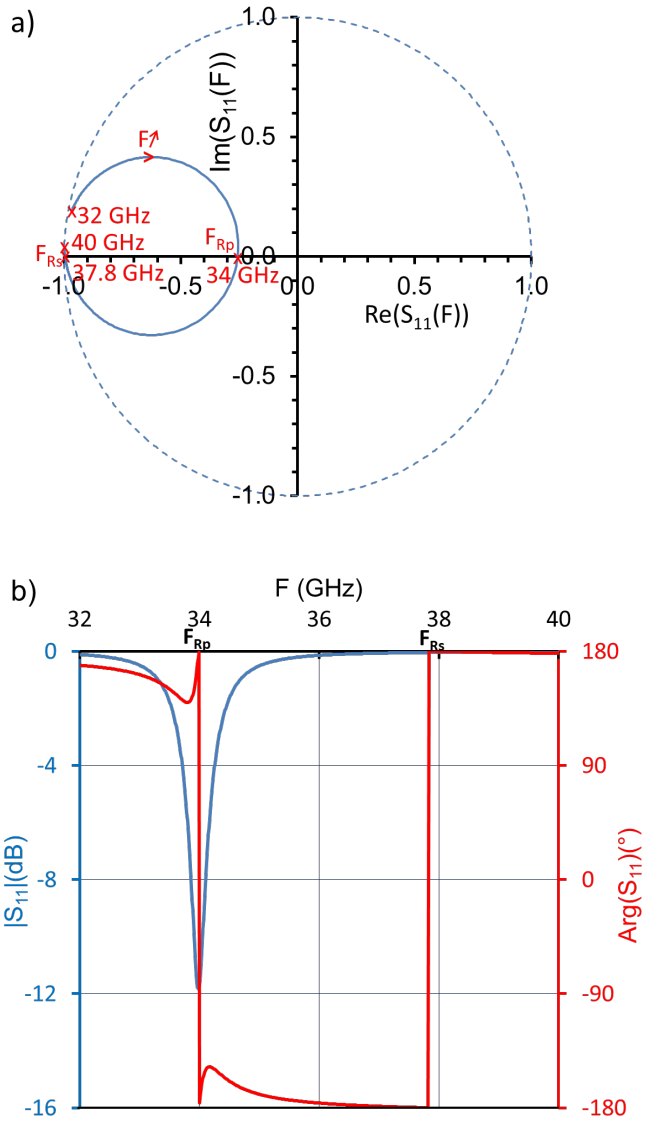


**FIGURE 2** (a) Polar plot (b) modulus (blue curve) and phase (red curve) of the reflection coefficient $S_{11}(F)$ versus frequency ($l = w$ = 2.5 mm, $p_l = p_w$ = 5 mm, $t$ = 50 µm, $\varepsilon'$ =3, $tg\delta$ = 0.014). $F_{Rp}$ and $F_{Rs}$ are the parallel and the series resonance frequencies.

it exhibits a parallel resonance ($F_{Rp}$) and a series resonance obtained with the inductance $L_s$. Moreover, each part of the proposed equivalent circuit is connected with a part of the structure (Fig. 1b) and has a physical meaning. Considering a mesh ($p_l$, $p_w$) of the structure, the RLC parallel circuit represents the part comprising the patch, the

dielectric layer and the ground plane. This circuit traduces the resonance phenomenon that occurs under the patch as mentioned in the section II. A parallel RLC circuit was already proposed in the literature for patch antennas or metasurfaces [40]- [42]. The $L_s$ inductance represents the complementary part of the mesh which is not metallized. As the dielectric presents low losses and low thickness compared to the wavelength, it is coherent to find this part equivalent to a low inductance $L_s$ (section V.B).

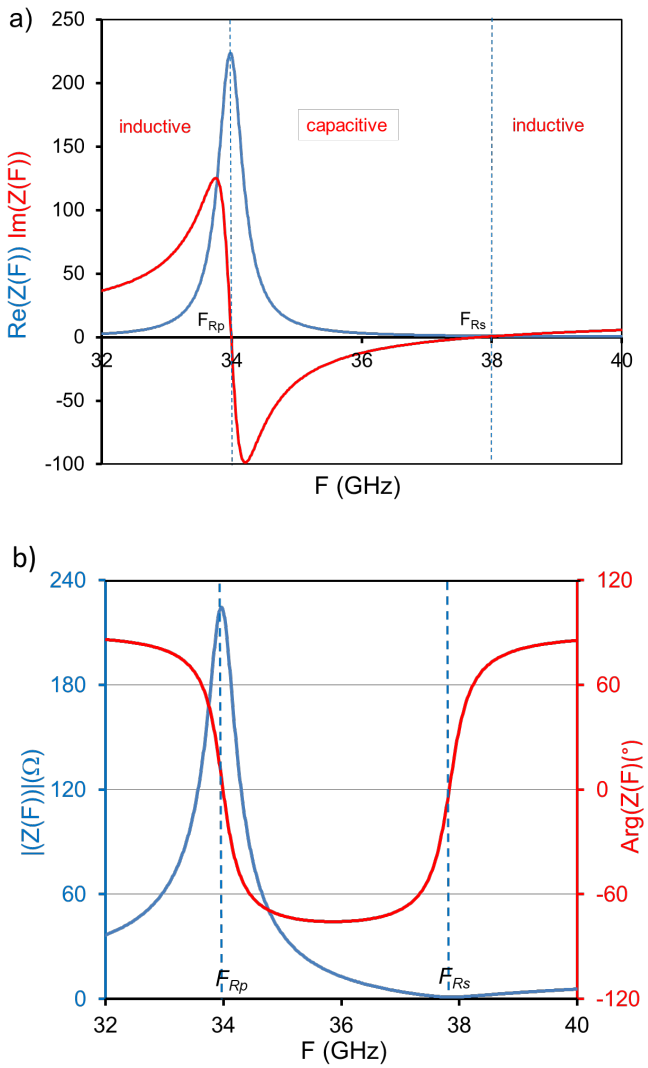


**FIGURE 3** Frequency evolutions of (a) the resistance (blue curve) and the reactance (red curve), (b) the modulus (blue curve) and the phase (red curve) of the surface impedance $Z(F)$ ($l = w = 2.5$ mm, $p_l = p_w = 5$ mm, $t = 50$. $\mu$m. $\varepsilon' = 3$, $tg\delta = 0.014$). $F_{Rp}$ and $F_{Rs}$ are the parallel and the series resonance frequencies.

The surface impedance of the mesurface is the sum of the impedances of each part :

$$Z(\omega) = R_Z(\omega) + jX_Z(\omega) = Z_{RLC}(\omega) + jL_s\omega \qquad (4)$$

The RLC circuit impedance $Z_{RLC}(\omega) = R_{RLC}(\omega) + j\,X_{RLC}(\omega)$ expresses as follow where the resonance angular frequency $\omega_{RLC}$ and the quality factor $Q_{RLC}$ were introduced :

$$Z_{RLC}(\omega) = \frac{jL\omega}{1 + j\frac{L}{R}\omega - LC\omega^2} = \frac{j\frac{R}{Q_{RLC}}\frac{\omega}{\omega_{RLC}}}{1 + j\frac{\omega}{Q_{RLC}\omega_{RLC}} - \frac{\omega^2}{\omega_{RLC}^2}} \qquad (5)$$

$$\omega_{RLC} = \frac{1}{\sqrt{LC}} \qquad (6)$$

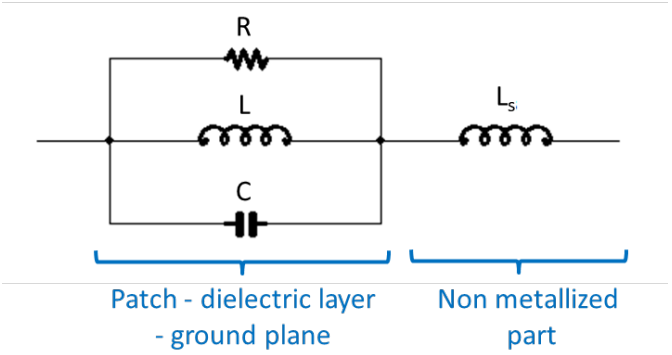


**FIGURE 4.** Equivalent circuit of the surface impedance Z(F) of the metasurface.

$$Q_{RLC} = RC\omega_{RLC} = \frac{R}{L\omega_{RLC}} = R\sqrt{\frac{C}{L}} = \frac{1}{tg\delta_{eff}} = Q_d \qquad (7)$$

$Q_{RLC}$ represents also the dissipative quality factor $Q_d$ of the metasurface [37], [38] which depends on the effective dielectric losses factor $tg\delta_{eff}$.

The expression (5) simplifies at the vicinity of the resonance frequency [41]:

$$\omega = \omega_{RLC} + \Delta\omega \qquad Z_{RLC}(\omega) \approx \frac{R}{1 + 2jQ_{RLC}\frac{\Delta\omega}{\omega_{RLC}}} \qquad (8)$$

The resistance $R_Z(\omega)$ of the impedance surface equals this of the RLC circuit and the $L_s$ inductance modifies the reactance $X_Z(\omega)$ :

$$R_Z(\omega) = R_{RLC}(\omega) = \frac{\frac{L^2\omega^2}{R}}{\frac{L^2\omega^2}{R^2} + (1 - LC\omega^2)^2} \qquad (9)$$

$$X_Z(\omega) = X_{RLC}(\omega) + L_s\omega = \frac{L\omega(1 - LC\omega^2)}{\frac{L^2\omega^2}{R^2} + (1 - LC\omega^2)^2} + L_s\omega \qquad (10)$$

The resonance frequency pulsation $\omega_{RLC}$ is the pulsation at which the resistance $R_Z(\omega)$ is maximum. This resistance equals to the resistance R of the equivalent circuit (9). At $\omega=\omega_{RLC}$, the surface impedance $Z(\omega_{RLC})$ writes :

$$Z(\omega_{RLC}) = R + jL_s\omega_{RLC} \qquad (11)$$

The imaginary part of this impedance gives the inductance $L_s$ :

$$L_s = \frac{X(\omega_{RLC})}{\omega_{RLC}} \qquad (12)$$

To determine the inductance L and the capacity C, the impedance $Z_{RLC}(\omega)$ is first deduced from $Z(\omega)$ in subtracting of the impedance of the $L_s$ inductance. Then, the quality factor $Q_{RLC}$ of the RLC circuit is obtained from (13) where the frequency bandwidth $\Delta F_Z$ corresponds to a decrease of

$|Z_{RLC}(\omega)|_{dB}$ of -3 dB around its maximum value $|Z_{RLC}(\omega_{RLC})| = R$ :

$$Q_{RLC} = \frac{F_{RLC}}{\Delta F_Z} \tag{13}$$

The inductance L and the capacity C are then deduced using (7).

The parallel $\omega_{Rp}$ and serial $\omega_{Rs}$ resonance angular frequencies can be expressed as a function of the circuit elements in considering that at the resonances, the reactance $X_Z(\omega)$ of the equivalent circuit vanishes. The relation (14) gives the analytical expression of $X_Z(F)$ establihed from (10) :

$$X_Z(\omega) = \frac{(L+L_s)\omega(1-LC\omega^2)(1-\frac{LL_s}{L+L_s}C\omega^2)+\frac{L_sL^2\omega^3}{R^2}}{\frac{L^2\omega^2}{R^2}+(1-LC\omega^2)^2} \tag{14}$$

A study of the influence of last term of the numerator of (14) shows that this term can be neglected. In this case, introducing the parallel $\omega_{Rp}$ and the series $\omega_{Rs}$ resonance angular frequencies, the reactance and the resistance of the surface impedance $X_Z(\omega)$ become:

$$R_Z(\omega) = \frac{\frac{L^2\omega^2}{R}}{\frac{L^2\omega^2}{R^2}+\left[1-(\frac{\omega}{\omega_{Rp}})^2\right]^2} \tag{15}$$

$$X_Z(\omega) = \frac{(L+L_s)\omega\left[1-(\frac{\omega}{\omega_{Rp}})^2\right]\left[1-(\frac{\omega}{\omega_{Rs}})^2\right]}{\frac{L^2\omega^2}{R^2}+\left[1-(\frac{\omega}{\omega_{Rp}})^2\right]^2} \tag{16}$$

where $$\omega_{Rp} = 2\pi F_{Rp} = \frac{1}{\sqrt{LC}} = \omega_{RLC} \tag{17}$$

$$\omega_{Rs} = 2\pi F_{Rs} = \frac{1}{\sqrt{(L\,//\,L_s)C}} \tag{18}$$

These resonance frequencies can also be determined in numerically solving $X_Z(F) = 0$.

The different steps of the data extraction for the previous example are detailed in Table I. Let's notice that as predicted the difference between $F_{RLC}$ and $F_{Rp}$ is not significant. The effective dielectric losses $tg\delta_{eff}$ obtained from the dissipative quality factor $Q_d$ is near of $tg\delta$.

The Fig. 5 presents the results obtained for the previous example of Fig. 2 and 3. The simulated and extracted data for the reflection coefficient and the surface impedance are compared showing that the curves superimposes with a good accuracy in all the frequency range. The case $L_s = 0$ is also presented showing that the series resonance frequency becomes infinite.

**TABLE I.** Different Steps of the Data Extraction and Extracted Data for the Example in Fig.2 and Fig.3.

| Steps | Extracted data |
|---|---|
| Full wave simulation | $S_{11}(F)$ |
| | $Z(F) = R_Z(F) + j\,X_Z(F)$ |
| Numerical solving of | $F_{Rp} = 33.98$ GHz |
| $X_Z(F) = 0$ | $F_{Rs} = 37.8$ GHz |
| Extraction of $R_Z(F)_{max}$ | $F_{RLC} = 33.98$ GHz |
| coordinates | $R = 223.6\ \Omega$ |
| $X_Z(F_{RLC}) = L_s\omega_{RLC}$ | $L_s = 58.8\ pH$ |
| | $\Delta F_Z = 454$ MHz |
| $\lvert Z_{RLC}(F)\rvert = \lvert Z(F) - jL_s\omega\rvert$ | $Q_{RLC} = Q_d = 74.8$ |
| | $tg\delta_{eff} = 1/Q_d = 0.0133$ |
| $Q_d = RC\omega_{Rp}$ | $C = 1.56$ pF |
| $F_{Rp} = 1/2\pi\sqrt{LC}$ | $L = 14$ pH |
| $\lvert S_{11}\rvert_{\min} = \left\lvert\frac{R-Z_0}{R+Z_0}\right\rvert$ | $\lvert S_{11}\rvert_{\min} = 0.26\ (-11.86\ dB)$ |
| $Q_r = Z_0C\omega_{Rp} = \frac{Z_0}{R}Q_d$ | $Q_r = 126.1$ |
| $Q_t = \frac{Q_dQ_r}{Q_d+Q_r}$ | $Q_t = 46.95$ |

The reflection coefficient $S_{11}(F)$ of the metasurface expresses as follow (4) :

$$S_{11}(F) = \frac{Z(F)-Z_0}{Z(F)+Z_0} \tag{19}$$

Using (8), this expression simplifies at the vicinity of the coefficient obtained at $\omega_{Rp}$, $Q_r$ and $Q_t$ are respectively the radiative and the total quality factors of the metasurface [40,41]:

$$\omega = \omega_{Rp} + \Delta\omega \qquad S_{11}(F) \approx \frac{S_{11\min} - 2jQ_t\frac{\omega-\omega_{Rp}}{\omega_{Rp}}}{1+2jQ_t\frac{\omega-\omega_{Rp}}{\omega_{Rp}}} \tag{20}$$

$$S_{11\min} = \frac{R-Z_0}{R+Z_0} = \frac{Q_d-Q_r}{Q_d+Q_r} \tag{21}$$

$$Q_r = \frac{Z_0}{R}Q_d = \frac{Z_0}{L\omega_{RLC}} = Z_0C\omega_{RLC} = Z_0\sqrt{\frac{C}{L}} \tag{22}$$

$$Q_t = \frac{Q_dQ_r}{Q_d+Q_r} = \frac{R\,//\,Z_0}{L\omega_{Rp}} = \frac{F_{Rp}}{\Delta F_{|S_{11}(F)|}} \tag{23}$$

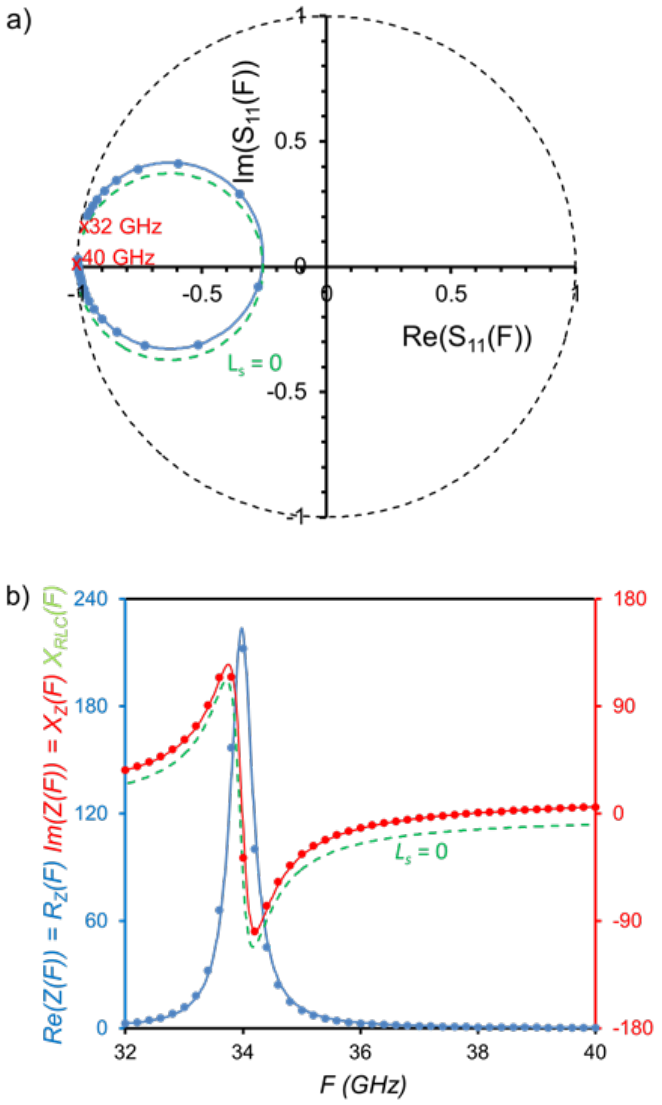


**FIGURE 5.** Comparison between Simulated (full lines) and Calculated Data (point markers) for (a) the Polar Plot of the Reflection Coefficient $S_{11}(F)$ as a function of frequency, (b) the Resistance $R_Z(F) = R_{RLC}(F)$ (blue curve), the Reactance $X_Z(F)$ (red curve) and the Reactance $X_{RLC}(F)$ (green dashed lines, case $L_s = 0$) ($h = w = 2.5$ mm, $p_l = p_w = 5$ mm, $t = 50$ $\mu$m, $\varepsilon = 3$, $tg\delta = 0.014$).

The relation (20) shows that, contrary to the impedance $Z(F)$, the reflection coefficient $S_{11}(F)$ is connected with the total quality factor $Q_t$ and to $S_{11min}$. The case of total absorption can be studied using these relations. The total absorption ($S_{11min} = 0$) is obtained for $R = Z_0$. In this case, the radiative quality factor $Q_r$ becomes equal to the dissipative quality factor $Q_d$ and the different quality factors and the absorption bandwidth expresses as follow [39] :

$$Q_t = \frac{Q_d}{2} = \frac{Q_r}{2} = \frac{1}{2tg\delta} \tag{24}$$

$$\Delta F_{|S_{11}(F)|} = 2tg\delta F_{Rp} \tag{25}$$

## V. FULLY ANALYTICAL MODEL OF A RECTANGULAR PATCH ARRAY METASURFACE

The next steps are to study the evolutions of the circuit elements values as a function of each geometrical and substrate parameters and to establish the analytical expressions of the circuit elements. For that, a large set of full wave simulations was carried out varying one single parameter around the values of the previous example. The values of the circuit elements were then extracted (previous section) and their evolutions as a function of each parameter were analyzed. The results about the R, L and C elements connected with the patch structure (section A) are first discussed and then those about the inductance $L_s$ (section B).

### *A. ANALYTICAL EXPRESSION OF THE RLC CIRCUIT ELEMENTS*

The evolutions of the $R$, $L$ and $C$ elements values as a function of the different parameters are reported in Fig. 6. The analysis of the results allows to distinguish four types of evolution as a function of the parameters: independent, linear, inversely linear and 1/square root evolutions as a function of the parameter (Table II). From these results, it is possible to give a first expression of the circuit elements where the vacuum permittivity, permeability and characteristic impedance were introduced:

$$R = k_R Z_0 \frac{tw}{\sqrt{\varepsilon_{eff}^{'}}\, tg\delta_{eff}\, p_l p_w} \tag{26}$$

$$L = k_L \mu_0 \frac{l_{eff} tw}{p_l p_w} \tag{27}$$

$$C = k_C \varepsilon_0 \frac{\varepsilon_{eff}^{'} l_{eff} p_l p_w}{tw} \tag{28}$$

The coefficients $k_L$, $k_C$ and $k_R$ are proportionality factors to determine. The following relations between the coefficients are obtained using the expressions of the resonance pulsation $\omega_{Rp}$ (17), the dissipative quality factor $Q_d$ (7) and the relations (26)-(28):

$$\omega_{Rp} = \frac{1}{\sqrt{LC}} = \frac{\pi c}{l_{eff}\sqrt{\varepsilon_{eff}^{'}}} \Rightarrow k_L k_C = \frac{1}{\pi^2} \tag{29}$$

$$Q_d = RC\omega_{Rp} = \frac{1}{tg\delta_{eff}} \Rightarrow k_R k_C = \frac{1}{\pi} \tag{30}$$

Two other relations can be obtained with the dissipative quality factor expressions (7) but they are not independent of (29) and (30):

$$Q_d = \frac{R}{L\omega_{Rp}} = R\sqrt{\frac{C}{L}} = \frac{1}{tg\delta_{eff}} \Rightarrow \frac{k_R}{k_L} = \pi,\ k_R\sqrt{\frac{k_C}{k_L}} = 1 \tag{31}$$

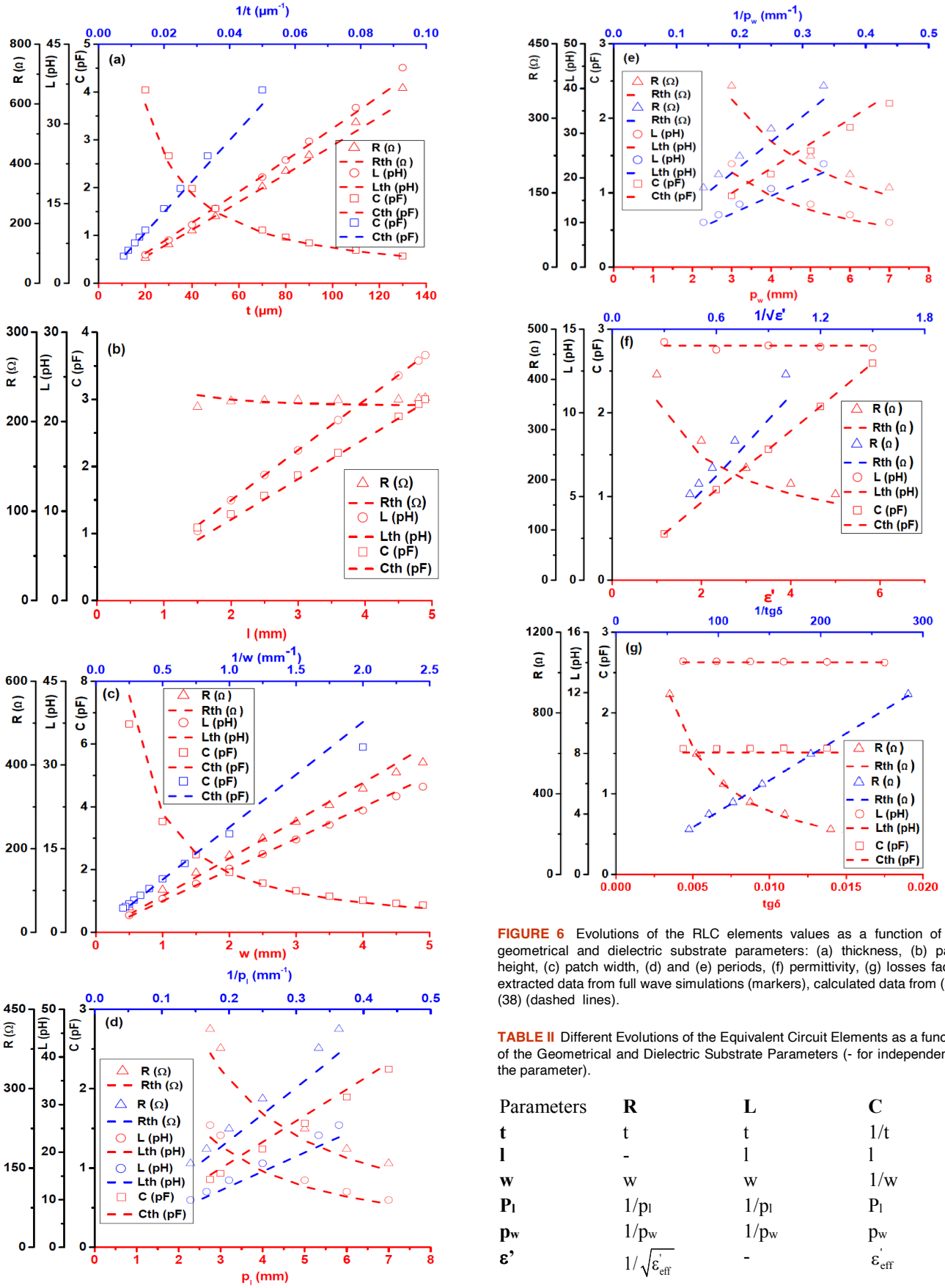


**FIGURE 6** Evolutions of the RLC elements values as a function of the geometrical and dielectric substrate parameters: (a) thickness, (b) patch height, (c) patch width, (d) and (e) periods, (f) permittivity, (g) losses factor, extracted data from full wave simulations (markers), calculated data from (36)-(38) (dashed lines).

**TABLE II** Different Evolutions of the Equivalent Circuit Elements as a function of the Geometrical and Dielectric Substrate Parameters (- for independent of the parameter).

| Parameters | **R** | **L** | **C** |
|---|---|---|---|
| **t** | t | t | 1/t |
| **l** | - | l | l |
| **w** | w | w | 1/w |
| **$P_l$** | $1/p_l$ | $1/p_l$ | $P_l$ |
| **$p_w$** | $1/p_w$ | $1/p_w$ | $p_w$ |
| **ε'** | $1/\sqrt{\varepsilon'_{eff}}$ | - | $\varepsilon'_{eff}$ |

**tgδ** 1/tgδ$_{eff}$ - -

To determine the coefficients $k_L$, $k_C$ and $k_R$, (26)-(28) are first rewritten using (29),(30) to keep only one coefficient k:

$$R = \frac{k}{\pi} Z_0 \frac{tw}{\sqrt{\varepsilon'_{eff}}\, tg\delta_{eff} p_l p_w} \quad (32)$$

$$L = \frac{k}{\pi^2} \mu_0 \frac{l_{eff} tw}{p_l p_w} \quad (33)$$

$$C = \frac{1}{k} \varepsilon_0 \frac{\varepsilon'_{eff} l_{eff} p_l p_w}{tw} \quad (34)$$

The value of this coefficient is adjusted to obtain the best fit between the extracted and the calculated circuit elements data all together. The following values of the different coefficients are obtained:

$$k = 8.8 \Rightarrow k_R = \frac{8.8}{\pi} \quad k_L = \frac{8.8}{\pi^2} \quad k_C = \frac{1}{8.8} \quad (35)$$

Finally, for the first resonance, the expressions of the R, L and C circuit elements of the analytical model are the following :

$$R = \frac{8.8}{\pi} \frac{Z_0 tw}{\sqrt{\varepsilon'_{eff}}\, tg\delta_{eff} p_l p_w} \quad (36)$$

$$L = \frac{8.8}{\pi^2} \mu_0 t \frac{l_{eff} w}{p_l p_w} \quad (37)$$

$$C = \frac{1}{8.8} \varepsilon_0 \varepsilon'_{eff} \frac{l_{eff}}{tw} p_l p_w \quad (38)$$

The elements circuit values calculated using (36)-(38) are compared to those extracted from full wave simulations in Fig. 6. A satisfying agreement between the data is obtained. These analytical expressions are sufficient to define the equivalent circuit of rectangular patch and/or mesh metasurfaces and so to determine their characteristics (the analytical expression of the $L_s$ inductance is discussed in the next section V.B). These expressions can be used to predict the influence of the different parameters on their frequency behavior and to perform frequency simulations. A complementary validation of the model is given in section VI. These expressions can be completed with those previously given of the parallel resonance angular frequency/frequency (17), (29) and of the different quality factors $Q_d$ (7), $Q_r$ (22) and $Q_t$ (23). The radiative $Q_r$ and total $Q_t$ quality factors can be expressed as a function of the geometry:

$$Q_r = \frac{Z_0}{R} Q_d = \frac{Z_0}{R tg\delta_{eff}} = \frac{\pi}{8.8} \frac{\sqrt{\varepsilon'_{eff}}\, p_l p_w}{tw} \quad (39)$$

$$Q_t = \frac{Z_0 // R}{R} Q_d = \frac{Q_d Q_r}{Q_d + Q_r} = \frac{\pi \sqrt{\varepsilon'_{eff}}\, p_l p_w}{8.8tw + \pi \sqrt{\varepsilon'_{eff}}\, p_l p_w tg\delta_{eff}} \quad (40)$$

As already mentioned, the parallel RLC resonant circuit corresponds to the part made of the patch, the dielectric substrate and the ground plane. At this step, in view to explain the origin of these expressions of the circuit elements (36)-(38), it is interesting to consider the equivalent electrical circuit of a single patch as the parallel association of an inductance $L_{patch}$, a capacity $C_{patch}$ and a resistance $R_{patch}$ and to introduce their expressions in these of R, L and C. These expressions are:

$$L_{patch} = \mu_0 t \frac{l_{eff}}{w} \quad (41)$$

$$C_{patch} = \varepsilon_0 \varepsilon'_{eff} \frac{l_{eff} w}{t} \quad (42)$$

$$R_{patch} = \frac{t}{\sigma_{eff}(\omega_{Rp}) l_{eff} w} = \frac{t}{\varepsilon_0 \varepsilon''_{eff} \omega_{Rp} l_{eff} w} \quad (43)$$

where $\sigma_{eff}(\omega_{Rp})$ represents the effective conductivity of the dielectric substrate (43). At the difference of $L_{patch}$ and $C_{patch}$ and due to the conductivity $\sigma_{eff}(\omega)$, the resistance $R_{patch}$ is frequency dependent. The value taken for $R_{patch}$ is that obtained for the parallel resonant angular frequency $\omega_{Rp}$ (29). Let's also notice that, the capacity $C_{patch}$ (42) and the resistance $R_{patch}$ (43) verify the relations (44) and (45) which apply to an empty capacity $C_0$ filled with a lossy dielectric:

$$C_{patch} = \varepsilon'_{eff} C_0 \quad \text{where} \quad C_0 = \varepsilon_0 \frac{l_{eff} w}{t} \quad (44)$$

$$R_{patch} = \frac{1}{\varepsilon''_{eff} C_0 \omega} = \frac{1}{tg\delta_{eff} C_{patch} \omega} \quad (45)$$

The expressions (41), (42) can be introduced in the first expressions of $L$ and $C$ (37), (38):

$$L = \frac{8.8}{\pi^2} L_{patch} \frac{w^2}{p_l p_w} \quad (46)$$

$$C = \frac{1}{8.8} C_{patch} \frac{p_l p_w}{w^2} \quad (47)$$

For the resistance $R$, introducing the parallel resonance angular frequency (29), the expression of $R_{patch}$ (43) becomes:

$$R_{patch}(\omega_{Rp}) = \frac{Z_0 t}{\pi \sqrt{\varepsilon'_{eff}}\, tg\delta_{eff} w} \quad (48)$$

Finally, the expression of $R$ is obtained after the introduction of the expression (48) in (36) :

$$R = k_R R_{patch}(\omega_{Rp}) \frac{w^2}{p_l p_w} = 8.8 R_{patch}(\omega_{Rp}) \frac{w^2}{p_l p_w} \quad (49)$$

The analytical expressions of the $R$, $L$ and $C$ elements are made of three parts: the proportionality factors $k_L$, $k_C$ and $k_R$ and two other terms connected respectively with the patch and the periodicity of the metasurface. From (46), (47) and

(49), the periodicity factors would be $\frac{w^2}{p_l p_w}$ for the inductance and the resistance, $\frac{p_l p_w}{w^2}$ for the capacity $C$. As the surface impedance is considered, it is logical to find similar periodicity factors for the inductance ($Z = jL\omega$) and the resistance ($Z = R$) and a reversed periodicity factor for the capacity($Z = 1/jC\omega$). However, these expressions are not in agreement with those proposed by different authors [23] where the periodicity factor is defined as the ratio of the surfaces of the considered part and of the mesh. For the patch, the periodicity factors would be $lw/p_l p_w$ for $R$ and $L$ and $p_l p_w/lw$ for $C$. A more complete study of the patch behavior under the incident electric field could explain this discrepancy. Similarly to $R_{patch}$ and $C_{patch}$, the analytical expressions of the resistance $R$ (49) and the capacity $C$ (47) verify the relations (44) and (45):

$$C = \varepsilon'_{eff} C_0 \text{ where } C_0 = \frac{1}{8.8}\varepsilon_0 \frac{l_{eff} p_l p_w}{tw} \tag{50}$$

$$R = \frac{1}{\varepsilon''_{eff} C_0 \omega_{Rp}} = \frac{1}{tg\delta_{eff} C \omega_{Rp}} \tag{51}$$

### *B. ANALYTICAL EXPRESSION OF THE Ls INDUCTANCE*

The evolutions of the extracted values of the inductance Ls are reported in Fig. 7 and the different observed evolutions as a function of the different parameters are grouped in Table III. Only two types of evolution are clearly observed: linear evolution of the inductance Ls as a function of the thickness t and of the patch geometry (Fig. 7a, 7b) and independence of Ls as a function of the substrate parameters (Fig 7d). The evolutions of the inductance Ls as a function of the periods are not obvious (Fig 7c). Moreover, similar values of Ls are obtained for the length l and the width w of the patch, the periods pl and pw and also the permittivity ε' and the losses factor tgδ (Fig. 7b, 7c and 7d). From these results, an analytical model was developed giving the expression of the Ls inductance and completing the previously presented model of the patch. The basic assumption is that the Ls inductance is connected with the non-metallized part of the mesh. This part is made of the dielectric layer and the ground plane. The behavior of such a configuration is well known: a part of the incident wave (polarized along Ox) propagates in the dielectric substrate where a standing wave appears resulting of multiple reflections at the interface air-dielectric and on the ground plane establishes. The relation giving the surface impedance noted Zd (d for dielectric) is [39]:

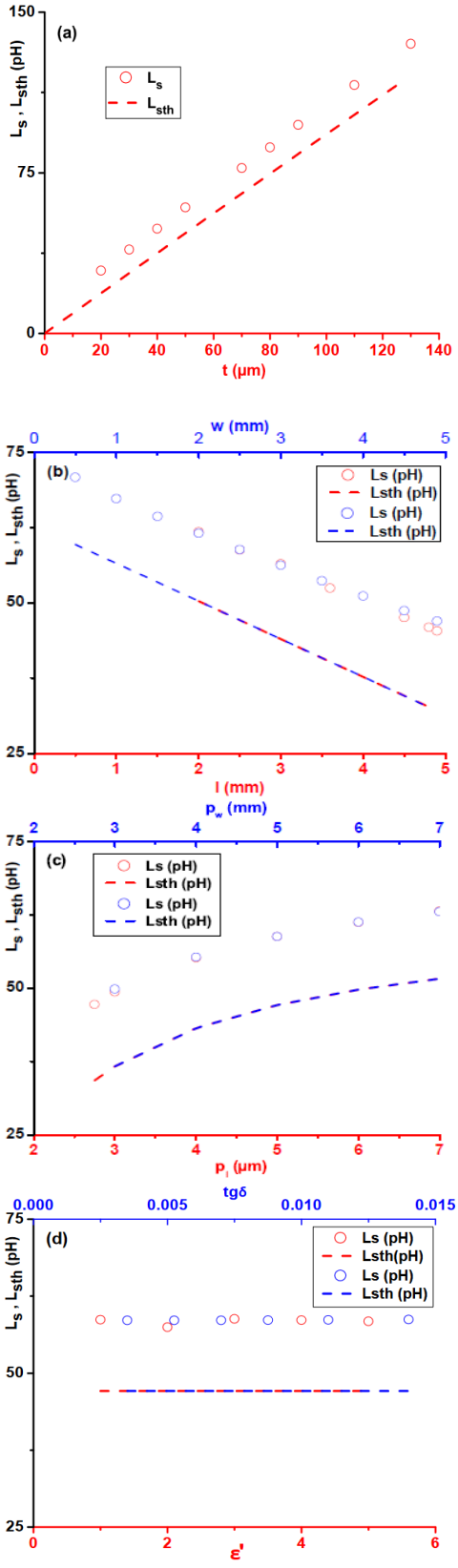


**FIGURE 7** Evolutions of the Ls Inductance Values Extracted from Full Wave Simulations as a function of the Different Parameters: a) thickness b) width and height of the patch c) periods d) permittivity and losses factor, extracted data from full wave simulations (markers), calculated data from the model (dashed curves).

**TABLE III** Different Evolutions of the $L_s$ Inductance as a Function of the Geometrical and Material Parameters (- for independent of the parameter).

| **Parameters** | ***Ls*** |
|---|---|
| *t* | *t* |
| *l, w,* | linearly decreasing |
| $p_l$,$p_w$ | undefined |
| $\varepsilon'$, $tg\delta$ | - |

$$Z_d = \frac{Z_0}{\sqrt{\varepsilon^*}} th(j\frac{2\pi}{\lambda_0}\sqrt{\varepsilon^*}t) = R_d + jX_d \quad (52)$$

In our specific case of low thickness and low losses of the substrate, the relation (52) simplifies and the surface impedance reduces to a surface inductance $L_d$ depending only of the thickness t of the substrate:

$$Z_d = jZ_0\frac{2\pi}{\lambda_0}t = jL_d\omega \quad \Rightarrow \quad L_d = \mu_0 t \quad (53)$$

As previously observed for the R, L and C elements (section V.A), for a periodic array metasurface, it is necessary to introduce the periodicity factor which is here the ratio of the surfaces of the non-metallized part ($p_l p_w$-$l_{eff}w$) and of the mesh ($l_{eff}w$). Finally, the surface inductance of the non-metallized part is expressed as:

$$L_s = \mu_0 t(\frac{p_l p_w - l_{eff}w}{p_l p_w}) = \mu_0 t(1-\frac{l_{eff}w}{p_l p_w}) \quad (54)$$

The predicted values of the inductance $L_s$ (54) are reported in Fig. 7 (dashed lines). The predicted evolutions of the $L_s$ inductance agree with those found from full wave simulations. The relation (54) explains the evolutions of the $L_s$ inductance as a function of all the parameters. However, a discrepancy is observed about the values of the $L_s$ inductance which are all higher than the calculated ones of a value $\Delta L_s$ of about 12 pH. This shift slightly decreases when one of the periods increases, has a reversed behavior with the patch dimensions and does not depend on the permittivity and the dielectric losses. An additional inductance would exist at the surface of the non-metallized part of the metasurface. In particular, it is not possible to confirm if the inductance Ls tends to zero at very low thickness.

Up to date, we have no clear explanation to propose about this additional inductance. A capacitive mutual coupling also exists between neighboring patches resulting in an additional capacity. This capacity is in parallel with the inductance $L_s$ and increases the apparent value of the inductance $L_s$. The value of this capacity can be estimated using the following relation established in [16] for square patches where g and p represent respectively the gap between two patches and the period:

$$C = \frac{p\varepsilon_0(\varepsilon'+1)}{\pi}\log(\frac{1}{\sin(\frac{\pi g}{2p})}) \quad (55)$$

The application of this relation to the example of section III (g = 2.5 mm) gives C = 10 fF. This value becomes 150 fF for g = 10 µm. So, this capacity is found too small to create the observed shift of the $L_s$ inductance value and the capacitive mutual coupling between neighboring patches is negligible. Other possibilities could be an additional inductance due to higher order evanescent modes [41] generated by the incident wave at the air-substrate interface or an inductive coupling effect between adjacent patches.

## VI. VALIDATION OF THE MODEL AND APPLICATIONS

### A. VALIDATION OF THE MODEL ON DIFFERENT STRUCTURES

In order to validate the model, the previous example and three structures with different geometry were studied. The results of the different COMSOL simulations and of the model are reported in Table IV. Compared to the example, the thickness is lower (25 µm) for the structures 1 and 2 and higher (120 µm) for the structure 3. The patches and the meshes are also rectangular (except structure 1 which has a square patch).

To take into account the fringing and the dispersion effects (see VIII-Appendix), the resonance frequencies and the circuit capacity and resistance are calculated for three different values of the permittivity: the substrate permittivity $\varepsilon'$, the low frequency eff ective permittivity $\varepsilon'_{eff\,0}$ and the permittivity $\varepsilon'_{eff}(F_{Rp})$ taking into the dispersion [42]. The extension of the patch length $\Delta l$ is also considered with the effective length $l_{eff}$ [40], [41].

Concerning the parallel resonance frequency, lower deviations between simulated and calculated data are obtained using $\varepsilon'$ or $\varepsilon'_{eff}(F_{Rp})$ permittivities. For the *R*, *L* and *C* circuit elements values, higher deviations are observed (maximum value 8.8 % for the resistance *R*). These results are satisfying if we consider that these results include possible errors introduced by full wave simulations and by the effective permittivity values. For the inductance $L_s$, the previously discussed shift in section V.B is observed.

### B. VALIDATION OF THE MODEL WITH A TWO PATCHES STRUCTURE

The model assumes that the equivalent circuit of the metasurface is made of the series connection of the equivalent circuit of each part of the mesh that are the patch and the non-metallized part of the mesh. To verify this, we propose to apply the model to a two patches metasurfaces. In this case, the expression (4) becomes:

$$Z(\omega) = Z_{RLC1}(\omega) + Z_{RLC2}(\omega) + jL_s\omega \quad (56)$$

Where $Z_{RLC1}(\omega)$ and $Z_{RLC2}(\omega)$ are the impedances of each patches (patch1 and patch2). The circuit elements

TABLE **IV** Comparison of the COMSOL Simulated Data (in red) and the Model Predictions (in blue) for Different Structures and Relative Errors in orange.

| Example | | | | | | | |
|---|---|---|---|---|---|---|---|
| ***t*** **(μm)** | ***l*** **(mm)** | $l_{eff}$ **(mm)** | ***w*** **(mm)** | $p_l$ **(mm)** | $p_w$ **(mm)** | $\varepsilon'$ | $tg\delta$ |
| 50 | 2.5 | 2.55 | 2.5 | 5 | 5 | 3 | 0.014 |
| | **COMSOL** | **Analytical model** | | | | | |
| | | $\varepsilon' = 3$ | | $\varepsilon'_{eff}(0) = 2.9$ | | $\varepsilon'_{FRp} = 2.95$ | |
| $F_{Rp}$ | 33.98 | 33.97 (-0.03) | | 34.57 (1.7) | | 34.25 (0.8) | |
| R | 223.6 | 217.75 (-2.62) | | 221.55 (-0.92) | | 219.55 (-1.8) | |
| L | 14 | 14.28 (2.0) | | | | | |
| C | 1.56 | 1.54 (-1.28) | | 1.49 (-4.49) | | 1.51 (-3.2) | |
| $L_s$ | 58.8 | 46.82 | | | | | |
| Structure 1 | | | | | | | |
| **t (μm)** | **l (mm)** | $l_{eff}$ **(mm)** | **w (mm)** | $p_l$ **(mm)** | $p_w$ **(mm)** | $\varepsilon'$ | tgδ |
| 25 | 2.5 | 2.52 | 2.5 | 5 | 4 | 4 | 0.02 |
| | **COMSOL** | **Analytical model** | | | | | |
| | | $\varepsilon' = 4$ | | $\varepsilon'_{eff}(0) = 3.92$ | | $\varepsilon'_{FRp} = 2.96$ | |
| $F_{Rp}$ | 29.75 | 29.72 (-0.1) | | 30.03 (0.9) | | 29.87 (0.4) | |
| R | 80.41 | 82.5 (2.6) | | 83.37 (3.7) | | 82.92 (3.1) | |
| L | 8.33 | 8.84 (6.1) | | | | | |
| C | 3.44 | 3.25 (-0.1) | | 3.18 (-7.6) | | 3.22 (-6.4) | |
| $L_s$ | 32.59 | 21.51 | | | | | |
| Structure 2 | | | | | | | |
| **t (μm)** | **l (mm)** | $l_{eff}$ **(mm)** | **w (mm)** | $p_l$ **(mm)** | $p_w$ **(mm)** | $\varepsilon'$ | tgδ |
| 25 | 2.0 | 2.02 | 4 | 4 | 6 | 4 | 0.02 |
| | **COMSOL** | **Analytical model** | | | | | |
| | | $\varepsilon' = 4$ | | $\varepsilon'_{eff}(0) = 3.99$ | | $\varepsilon'_{FRp} = 3.95$ | |
| $F_{Rp}$ | 36.91 | 37.06 (0.4) | | 37.11 (0.5) | | 37.31 (1.1) | |
| R | 105.26 | 110 (4.5) | | 110.15 (4.6) | | 110.74 (5.2) | |
| L | 8.82 | 9.45 (7.1) | | | | | |
| C | 2.11 | 1.95 (-7.6) | | 1.95 (-7.6) | | 1.93 (-8.5) | |
| $L_s$ | 32.26 | 20.82 | | | | | |
| Structure 3 | | | | | | | |
| **t (μm)** | **l (mm)** | $l_{eff}$ **(mm)** | **w (mm)** | $p_l$ **(mm)** | $p_w$ **(mm)** | $\varepsilon'$ | tgδ |
| 120 | 2.0 | 2.11 | 3 | 4 | 6 | 4 | 0.02 |
| | **COMSOL** | **Analytical model** | | | | | |
| | | $\varepsilon' = 4$ | | $\varepsilon'_{eff}(0) = 3.77$ | | $\varepsilon'_{FRp} = 3.92$ | |
| $F_{Rp}$ | 35.66 | 35.52 (-0.4) | | 36.77 (3.1) | | 35.87 (0.6) | |
| R | 434.3 | 396 (-8.8) | | 409.9 (-5.6) | | 399.9 (-7.9) | |
| L | 35.83 | 35.48 (-1.0) | | | | | |
| C | 0.56 | 0.57 (1.8) | | 0.57 (1.8) | | 0.53 (-5.4) | |
| $L_s$ | 126 | 111 | | | | | |

expressions are those previously established in section V.A (36)-(38). The expression of the Ls inductance becomes:

$$L_s = \mu_0 t\left(\frac{p_l p_w - l_{1eff} w_1 - l_{2eff} w_2}{p_l p_w}\right) \tag{57}$$

It is expected to observe two absorptions in the studied frequency range. For comparison, COMSOL simulations were performed for the Metasurfaces comprising the two patches (patch1 and patch2), the patch1 only and the patch2 only. Patches are square with different sides: $l_1 = w_1 = 2.5$ mm and $l_2 = w_2 = 2.2$ mm. All other parameters are similar to these of the previously studied example. The modulus of the reflection coefficients as a function of the frequency are compared in Fig.8 for the different structures. The model predictions are also reported (56), (57). From Fig.8, we can notice a good agreement between simulated and calculated data showing the validity of the model. The resonance frequencies observed with the model are slightly higher than the simulated ones (maximum deviation + 1.7%). A reversed behavior is observed for the maximum absorptions (maximum deviation -0.5 dB).

The use of several different patches in the periodic mesh is of interest in view of applications for example absorbers. Such structures allow to consider several different absorptions (absorption frequency and absorption level) in a given frequency range. These absorptions can be chosen narrow and spaced to select specific frequencies or juxtaposed to broaden the absorption frequency band.

### *C. APPLICATION TO PERFECT ABSORBERS*

The model predicts that the resistance *R* does not depend on the patch length (relation (36)). Only a slight decrease is observed from full wave simulations (Fig. 6b). On the other hand, the resistance *R* increases linearly with the patch width (Fig. 6c). So, acting on these 2 parameters, it is possible to adjust independently the resonance frequency and the absorption level of the metasurface. This property has been used for patch antennas design. The total absorption condition is obtained from relation (36) in the case $R = Z_0$:

$$8.8\frac{tw}{\pi\sqrt{\varepsilon'_{eff}}\, tg\delta_{eff}\, p_l p_w} = 1 \tag{58}$$

All the parameters of relation (58) can be used to obtain the total absorption alone or with others. In particular, it can be obtained by adjusting the width w of the patch (rectangular patch). The optimum width value $w_{opt}$ to obtain the total absorption is deduced from the relation (58):

$$w_{opt} = \frac{\pi\sqrt{\varepsilon'_{eff}}\, tg\delta_{eff}\, p_l p_w}{8.8t} \tag{59}$$

As an example, we propose to change the width of the previously studied two patches metasurface to obtain two total absorptions in the studied frequency range. As expected, the relation (59) gives similar values of the width for the patch's length:

$$w_{patch1} = 4.18 \text{ mm} \quad w_{patch2} = 4.12 \text{ mm} \tag{60}$$

The COMSOL simulation and the model predictions of the modified metasurface are presented in Fig. 9. These results show that, as predicted, the structure has now become a two patches structure with two total absorptions.

## VII. CONCLUSIONS

This work presents a fully analytical circuit-based model of low thickness and rectangular patch/mesh metasurfaces.

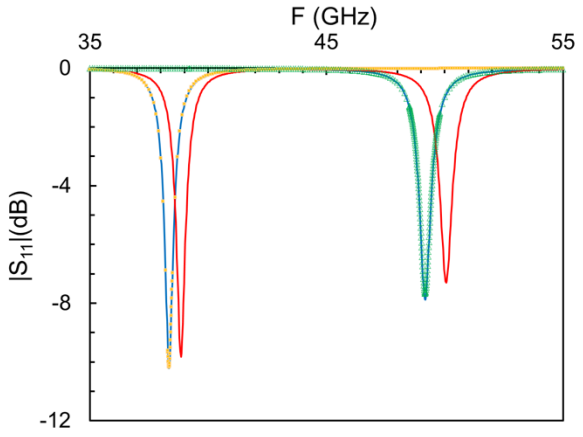


**FIGURE 8** COMSOL simulated $|S_{11}(F)|_{dB}$ for the two patches (blue line), patch1 only (yellow squares), patch2 only (green crosses) metasurfaces, the model predictions for the two patches metasurface (red line), ($h_1 = w_1 = 2.2$ mm, $h_2 = w_2 = 1.7$mm, $p_l = p_w = 5$ mm, t = 50 $\mu$m, $\varepsilon' = 3$, $tg\delta = 0.014$).

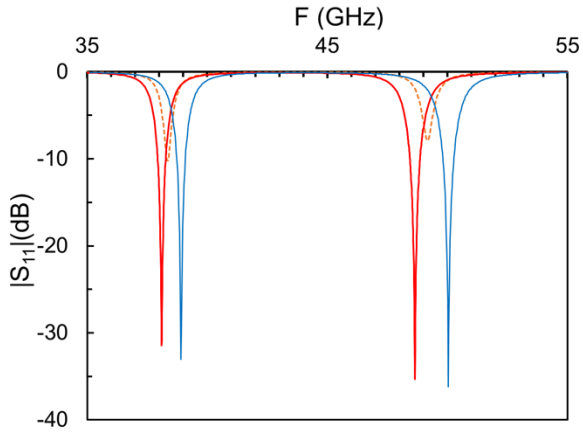


**FIGURE 9** COMSOL simulated $|S_{11}(F)|_{dB}$ for the total absorbing two patches metasurface (blue line), the model predictions (red line) and the previous two patches metasurface (yellow dashed line), ($h_1 = 2.2$ mm, $w_1 = 4.18$ mm, $h_2 = 1.7$mm, $w_2 = 4.12$ mm, $p_l = p_w = 5$ mm, t = 50 $\mu$m, $\varepsilon' = 3$, $tg\delta = 0.014$).

The model is elaborated in two steps on the basis of full wave simulations (wave simulations (COMSOL software). First, the surface impedance and the equivalent circuit are deduced from the frequency evolution of the reflection coefficient. Secondly, the analytical expressions of the circuit elements were established from the analysis of their evolutions as a function of the geometrical and substrate parameters. The expressions of the quality factors are also obtained. Contrary to previous works on such metasurfaces with higher thickness, the absorption corresponds to the first resonance under the patch which behaves as a resonator and the electric field is orientated perpendicular to the incident electric field. The equivalent circuit is a parallel RLC resonant circuit in series with an inductance $L_s$. The parallel RLC circuit represents the part comprising the patch, the dielectric layer and the ground plane. The impedance of this resonant circuit expresses as the product of a proportionality factor, the impedance of a single patch and a periodicity factor. The $L_s$ inductance is connected with the complementary part of the mesh. Its value depends of the dielectric layer thickness and of a periodicity factor.

The model is validated on different examples which a two patches metasurface. Specific properties are evidenced like the influence of the periodicity, the quasi-independence of the equivalent circuit resistance versus the height of the patch, the possible extension of the model to multi-patches structures. The total absorption condition is established and an example of application is given adjusting the width of the patch. This model is useful in view of new applications development notably electrically driven tunable metasurfaces which need low thickness.

## VIII. APPENDIX: ANALYTICAL EXPRESSION OF THE EFFECTIVE PARAMETERS OF THE MICROSTRIP LINE

The effective parameters of the microstrip line introduced in the model are the effective length $l_{eff}$ of the patch, the effective permittivity $\varepsilon'_{eff}$ and the effective losses factor $tg\delta_{eff}$.

They are involved in key quantities such as the parallel resonance frequency $F_{Rp}$ (6,33) and the $R$, $L$ and $C$ elements of the equivalent circuit (39-41). They are introduced to consider the fringing effects occurring in the cross section ( $\varepsilon'_{eff}$ ) and at each edge of the patch (edge effects, $l_{eff}$). There have been numerous investigations to establish analytical expressions of these parameters [40-46]. We have retained the expressions (60-67). The expressions (61), (62) give the effective length of the microstrip line [40-41]. The increase of the length $\Delta l$ depends on the permittivity and the thickness of the substrate and on the width of the patch. The model needs also the value of the effective permittivity at the resonance frequency $F_{Rp}$. This calculation is made in two steps. First, the low frequency effective permittivity $\varepsilon'_{eff\,0}$ and the characteristic impedance $Z_{c0}$ of the microstrip line are obtained from relations (63) which only apply in the case of a substrate thickness lower than the width of the patch [42]. As the frequency increases, the dispersion phenomenon appears [43-45]. The effective permittivity increases with frequency to be equal to the permittivity of the substrate at very high frequency. So, secondly, the dispersion is considered with the model of Hammerstad-Jansen [46] which is qualified of simple and accurate. The permittivity $\varepsilon'_{eff}(F_{Rp})$ is determined using relations (63)-(66) [42]. In this model, the frequency $F_t$ represents the cutting frequency of the first mode.

$$l_{eff} = l + 2\Delta l \tag{61}$$

$$\Delta l = \frac{0.412(\varepsilon' + 0.3)(\frac{w}{t} + 0.264)}{(\varepsilon' - 0.258)(\frac{w}{t} + 0.8)} t \tag{62}$$

$$\frac{w}{t}>1 \quad \begin{cases} \varepsilon'_{eff0} = \dfrac{1+\varepsilon'}{2} + \dfrac{\varepsilon'-1}{2}(1+12\dfrac{t}{w})^{-1/2} \\ Z_{c0} = \dfrac{Z_0/\sqrt{\varepsilon'_{eff0}}}{\dfrac{w}{t}+1.393+0.667\ln(\dfrac{w}{t}+1.444)} \end{cases} \tag{63}$$

$$F_t = \frac{Z_{c0}}{2\mu_0 t} \tag{64}$$

$$\varepsilon'_{eff}(F) = \varepsilon' - \left[ \frac{\varepsilon' - \varepsilon'_{eff0}}{1+\dfrac{\varepsilon'_{eff0}}{\varepsilon'}(\dfrac{F}{F_t})^2} \right] \tag{65}$$

The effective dielectric losses factor $tg\delta_{eff}$ can be evaluated in extending the relations (63-65) to the case of a complex effective permittivity. For that the permittivity ε' is replaced by the complex permittivity $\varepsilon^* = \varepsilon'-j\varepsilon''$ in these expressions [47]. The effective dielectric losses are then calculated using (66) and (67). In our case, the deviation between $tg\delta_{eff}$ and $tg\delta$ is found very small.

$$tg\delta_{eff0} = \frac{\varepsilon''_{eff0}}{\varepsilon'_{eff0}} \tag{66}$$

$$tg\delta_{eff}(F_{Rp}) = \frac{\varepsilon''_{eff}(F_{Rp})}{\varepsilon'_{eff}(F_{Rp})} \tag{67}$$

## IX. REFERENCES

[1] T. J. Cui, D. Smith, R. Liu, "Metamaterials: Theory, Design, and Applications", Boston, MA, USA Springer, 2010.
[2] F. Capolino, "Theory and Phenomena of Metamaterials", CRC press, 2017.
[3] K.Achouri, C. Caloz, "Electromagnetic Metasurfaces: Theory and Applications", IEEE Press, John Wiley & Sons, 2021.
[4] A. Li, S. Singh, D. Sievenpiper, "Metasurfaces and their applications", Nanophotonics, vol. 7, no. 6, pp. 989-1011, 2018.
[5] S.B. Glybovski, S. A. Tretyakov, P. A. Belov, Y. S. Kivshar, C. R. Simovski, "Metasurfaces: from microwaves to visible", Science Direct, Physics Reports, vol. 634, pp. 1-72, 2016.
[6] S. Sun, Q. He, J. Hao, S. Xiao, L. Zhou, "Electromagnetic metasurfaces: physics and applications". Advances in Optics and Photonics, vol. 11, no. 2, June 2019.
[7] T.K. Wu, "Frequency Selective Surface and Grid Array", Wiley, New York, 1995.
[8] B.A. Munk, "Frequency Selective Surface: Theory and Design", Wiley, New York, 2000.
[9] R.S. Anwar, L. Mao, H. Ning, "Frequency selective surfaces: a review", https://www.mdpi.com/2076-3417/8/9/1689.
[10] F. Costa, A. Monorchio, G. Manara, "An overview of equivalent circuit modeling techniques of frequency selective surfaces and Metasurfaces", The Applied Computational Electromagnetics Society Journal (ACES), 960-976, 2014.
[11] D. Sievenpiper, "High impedances electromagnetic ground planes", Ph.D; thesis, Univ. Calif., Los Angeles, CA, 1999.
[12] D. Sievenpiper, L. Zhang, E. Yablonovitch, "High impedances electromagnetic ground planes", IEEE MTT-S Intl. Microwave Symp, Anaheim, CA, 1999.
[13] D. Sievenpiper, L. Zhang, R.F.J. Broas, N.G. Alexopoulous, E. Yablonovitch, "High-impedance electromagnetic surface with a forbidden frequency band", IEEE Trans. Microwave Theory Technics, vol.47, no. 11, pp. 2059-74, 1999.
[14] C. R. Simovski, A.A. Sochava, "High-impedance surfaces based on self-resonant grids. Analytical modelling and numerical simulations", Progress In Electromagnetics Research, Prog. Electromagn. Res. PIER43, 239–256, 2003.
[15] S.A. Tretyakov, C.R. Simovski, "Dynamic model of artificial reactice impedance surfaces", J. of Electromagn., Waves and Appl., vol. 17, No.1, 131-145, 2003.
[16] S.A. Tretyakov, "Analytical Modeling in Applied Electromagnetics", Artech House, Boston, 2003
[17] C. R. Simovski, P. de Maagt, I. V. Melchakova, "High-impedance surfaces having stable resonance with respect to polarization and incidence angle", IEEE Transactions on Antennas and Propagation, vol. 53, no. 3, pp. 908-914, March 2005, doi: 10.1109/TAP.2004.842598.
[18] O. Luukkonen, C.R. Simovski, G. Granet, G. Goussetis, D. Lioubtchenko, A.V. Räisänen, S.A. Tretyakov, "Simple and accurate analytical model of planar grids and high-impedance surfaces comprising metal strips or patches", IEEE Trans. on Antennas and Propagation, vol.56, no.6, pp. 1624-1632, 2008.
[19] M. Hosseini, M. Hakkak, "Characteristics estimation for Jerusalem cross-based artificial magnetic conductors", IEEE Antennas and Wireless Propagation Letters, vol. 7, 58-61, 2008.
[20] O. Luukkonen, F. Costa, C.R. Simovski, A. Monorchio, S.A. Tretyakov, "A thin electromagnetic absorber for wide incidence angles and both polarizations", IEEE Trans. on Antennas and Propagation, vol.57, no.10, pp. 3119-3125, 2009.
[21] A.K. Azad, W.J.M. Kort-Kamp, M. Sykora, N.R. Weisse-Bernstein, T.S. Luk, A.J. Taylor, D.A.R. Dalvit, H.T. Chen, "Metasurface broadband solar absorber", Sci. Rep. **6**, 20347 (2016), doi.org/10.1038/srep20347.
[22] F. Costa, A. Monorchio and G. Manara, "Analysis and design of ultra-Thin electromagnetic absorbers comprising resistively loaded high impedance surface", IEEE Transactions on Antennas and Propagation, vol. 58, no. 3, pp. 1201-1209,2013, doi: 10.1109/TAP.2012.2227923.
[23] F. Costa, S. Genovesi, A. Monorchio and G. Manara, "A circuit-based model for the interpretation of perfect metamaterial absorbers", IEEE Transactions on Antennas and Propagation, vol. 61, no. 3, pp. 1201-1209,2013, doi: 10.1109/TAP.2012.2227923.
[24] N. I. Landy, S. Sajuyigbe, J. J. Mock, D. R. Smith, W. J. Padilla, "Perfect metamaterial absorber", Phys. Rev. Lett., vol. 100, May 2008.
[25] S. Zahra, L. Ma, W. Wang, et al., Electromagnetic metasurfaces and reconfigurable metasurfaces: a review. Frontiers in Physics, 2021, vol. 8, p. 593411.
[26] L. Shao, J. Zhang, I. D. Rukhlenko, W. Zhu. "Electrically reconfigurable microwave metasurfaces" [Invited] J. Chinese Optics Letters, 2022, 20(10: 103601.
[27] P. Yaghmaee, O. Hamza Karabey, B. Bates, C. Fumeaux, R. Jakoby, "Electrically tuned microwave devices using liquid crystal technology", International Journal of Antennas and Propagation, vol. 2013, Article ID 824214, 9 pages, 2013, doi.org/10.1155/2013/824214.
[28] J. Xu, R. Yang, Y. Fan, Q. Fu, F. Zhang, "A review of tunable electromagnetic metamaterial with anisotropic liquid crystals", Frontiers in physics, 9, 2021, 633104, doi: 10.3389/fphy.2021.633104.
[29] N. Tentillier, F. Krasinski, R. Sauleau, B. Splingart, H. Lhermite, Ph. Coquet, "A liquid crystal, tunable, ultra-thin Fabry-Perot resonator in Ka Band", IEEE Antennas and Wireless Propagation Letters, 8, 701-704, 2009.
[30] F. Zhang, Q. Zhao, W. Zhang, J. Sun, J. Zhou, D. Lippens, "Voltage tunable short wired pair type of metamaterial infiltrated by nematic liquid crystals", Appl. Phys. Lett., 97, 134103, 2010.
[31] F. Zhang, W. Zhang, Q. Zhao, J. Sun, K. Qiu, J. Zhou, D. Lippens, "Electrically controllable fishnet metamaterial based on nematic liquid crystal", Optics Express, 19, 2, pp. 1563-1568, 2011.
[32] F. Costa, A. Monorchio,G. Manara, "An equivalent-circuit modeling of high impedance surfaces employing arbitrarily shaped FSS" In: 2009 International, Conference on Electromagnetics in Advanced Applications. IEEE, 2009. p. 852-855.
[33] A. Sellier, T. V. Teperik, A. de Lustrac, "Resonant circuit model for efficient metamaterial absorber", Optics Express, vol. 21, Issue S6, pp. A997-A1006 (2013), doi.org/10.1364/OE.21.00A997.
[34] J. Sarrazin, A. C. Lepage, X. Begaud, « High-impedance surface design considerations", IEEE Antennas and Propagation Symposium, Jun 2012, Chicago, United States. pp.3569 - 3572, 10.1109/APS.2004.1330117. hal-00983587.

[35] C. Caloz, T. Itoh, “Electromagnetic Metamaterials Transmission Line: Theory and Microwave Applications”, John Wiley & Sons, 2005.
[36] R. Rodríguez-Berral, F. Mesa F. Medina, "Analytical multimodal network approach for 2-D arrays of planar patches/apertures embedded in a layered medium,", IEEE Transactions on Antennas and Propagation, vol. 63, no. 5, pp. 1969-1984, May 2015, doi: 10.1109/TAP.2015.2406885.
[37] F. Mesa, R. Rodriguez-Berral, F. Medina, "Unlocking complexity using the ECA: The equivalent circuit model as an efficient and physically insightful tool for microwave engineering," , IEEE Microwave Magazine, vol. 19, no. 4, pp. 44-65, June 2018, doi: 10.1109/MMM.2018.2813821.
[38] N. Fernez, L. Burgnies, J. Hao, C. Mismer, G. Ducourneau, D. Lippens, "Radiative quality factor in thin resonant metamaterial absorbers", IEEE Transactions on Microwave Theory and Techniques, vol. 66, no. 4, pp. 1764-1772, 2018, doi: 10.1109/TMTT.2017.2784808
[39] D.M. Pozar, “Microwave Engineering”, John Wiley & Sons, 4th edition, 2011.
[40] C.A.. Balanis, “Antenna theory: Analysis and Design”, John Wiley & Sons, Inc. NY, 1997.
[41] Y. T. Lo, S. W. Lee, “Antenna handbook: theory, applications, and design”, Chap. 10, “Microstrip antennas”, edited by Y.T Lo, S.W. Lee, Van Nostrand Reinhold New York, 1988.
[42] C.A. Balanis, “Advanced engineering electromagnetics”, Chapter 8, “Strip line and Microstrip lines”, John Wiley & Sons, 2nd edition, 1989
[43] A.K. Verma, R. Kumar, "A new dispersion model for microstrip line", IEEE Transactions on Microwave Theory and Techniques, vol. 46, no. 8, pp. 1183-1187, Aug. 1998, doi: 10.1109/22.704966.
[44] M.N. O. Sadiku, S. M. Musa, S.R. Nelatury, "Comparison of dispersion formulas for microstrip lines", IEEE Southeast Con, 2004. Proceedings., Greensboro, NC, USA, 2004, pp. 378-382, doi: 10.1109/SECON.2004.1287946.
[45] M.V. Schneider, “Microstrip dispersion”, Proc. IEEE, 60, no1, 144-146, Jan 1972.
[46] E.O. Hammerstad, “Equations for microstrip circuit design”, Proc. Fifth European Microwave Conf., 268-272, September 1975.
[47] J. Hinojosa, “Contribution à la caractérisation électromagnétique de matériaux à partir de lignes plaquées - applications à l’étude de nouveaux matériaux”, Ph.D. thesis, Univ. Lille, France, May 1995.